GFZ
POTSDAM

Originally published as:

Quesnel, Y., Sotin, C., Langlais, B., Costin, S., Mandea, M., Gottschalk, M., Dyment, J. (2009): Serpentinization of the martian crust during Noachian. - Earth and Planetary Science Letters, 277, 1-2, 184-193

DOI: 10.1016/j.epsl.2008.10.012

Serpentinization of the Martian crust during Noachian

Yoann Quesnel[1,*], Christophe Sotin[2,3], Benoit Langlais[3,4], Simona Costin[5], Mioara Mandea[1], Matthias Gottschalk[1], Jérome Dyment[6]

1- GeoForschungsZentrum Potsdam, Telegrafenberg, 14473 Potsdam, Germany

2- Jet Propulsion Laboratory, California Institute of Technology, Pasadena, California, USA

3- CNRS, UMR 6112, Laboratoire de Planétologie et Géodynamique de Nantes, 2, rue de la Houssinière, 44322 Nantes, France

4- Université de Nantes, Laboratoire de Planétologie et Géodynamique de Nantes, 2, rue de la Houssinière, 44322 Nantes, France

5- Department of Geological Sciences, University of Saskatchewan, 114, Science Place, Saskatoon, SK, S7N 5E2, Canada

6- Institut de Physique du Globe de Paris, Géosciences Marines, 75252 Paris, France

*Corresponding author. Tel.: +49 331 288 1270; fax: +49 331 288 1235

E-mail address: quesnel@gfz-potsdam.de (Y. Quesnel)

Abstract:

This paper describes a model of serpentinization of the Southern Martian crust that may explain the topographic dichotomy, the absence of an associated free-air gravity anomaly and the presence of strong magnetic anomalies in the Southern Hemisphere. The thermodynamical conditions for serpentinization were likely met in the lithosphere during the Noachian period. This process may have decreased the density in the Southern crust and created the topographic dichotomy. Different reactions of serpentinization that can form magnetite have been considered. Assuming an intense magnetic field (core dynamo), we obtain chemical remanent magnetizations that are in the order of the estimates deduced from Martian magnetic anomaly studies. The pertinence and the implications of our model concerning the early thermal evolution of Mars are discussed, with emphasis on the intensity of the paleo-magnetic field.

Keywords: Mars, serpentinization, dichotomy, magnetization, Noachian, early evolution, magnetite

1. Introduction

Most of the processes that shaped Mars occured during the Noachian era (4.5-3.7 Ga). The Martian dichotomy - between a cratered, high and magnetic Southern Hemisphere and a flat, low and demagnetized Northern Hemisphere (Figure 1) - was probably formed during this period. Most of the magnetic anomalies revealed by the MAGnetometer/Electron Reflectometer (MAG/ER) experiment onboard the Mars Global Surveyor (MGS) probe are predominantly distributed in the Southern Hemisphere over Noachian surfaces, which argues in favor of a global dynamo field that ceased before the end of this period (Acuña et al., 2001). To explain the absence of magnetic anomalies over the Northern Hemisphere, the origin of this dichotomy has to be investigated. Exogenic (crustal thinning by one or several impacts) and/or endogenic (degree-1 mantle convection) were suggested (see Watters et al., 2007 and references therein). Via a single or several long-lived hot plumes, the growth of the Tharsis volcanic province was probably initiated during Noachian (Roberts and Zhong, 2007; Solomon et al., 2005). Some of its associated volcanic units are then emplaced on old magnetized crust, whereas others may have erased the crustal magnetization during their post-dynamo emplacement. A key issue is then to propose a scenario that explains all these planetary-scale geological features, considering the timing of the cessation of the core dynamo.

This can be investigated by studying the crustal magnetic field anomalies observed by the MGS MAG/ER instrument. Models dealing with the Martian crustal magnetization predict intense and deep sources, in comparison with the Earth's crustal magnetization (Langlais et al., 2004; Quesnel et al., 2007; Whaler and Purucker, 2005). This gives some information about the material and the geological processes involved in this remanent magnetization. Before presenting the arguments which favor

54 magnetite (Fe_3O_4) as main magnetization carrier, we review other potential candidates. Pyrrhotite (FeS)
55 was suggested because it was observed in SNC meteorites; it also explains the apparent
56 demagnetization of impact basins (Rochette et al., 2001). Pyrrhotite would imply a relatively thin
57 magnetized layer due to its low Curie temperature. Multi-domain hematite (Fe_2O_3) was also invoked
58 because it can be associated with large TRM (Kletetschka et al., 2000, 2005). However, the localized
59 hematite spherules of Sinus Meridiani are mostly composed of single-domain hematite (Morris et al.,
60 2005), associated with much lower magnetization. Furthermore, hematite minerals are more readily
61 weathered compared to magnetite. In conclusion, magnetite appears to be the most serious candidate as
62 magnetization carrier. Together with maghemite, its oxydation product, it composes most of the
63 magnetic phase on soils and rocks of Spirit landing sites (Bertelsen et al., 2004). Its high Curie
64 temperature and its stable remanence may also explain the large magnetization depths derived from
65 MGS magnetic measurements (Arkani-Hamed, 2005a; Quesnel et al., 2007).

66 The preferred Martian crustal magnetization mechanism is thermo-remanent magnetization
67 (TRM): minerals cool below their Curie temperature in the presence of a dynamo field during seafloor
68 spreading (Connerney et al., 1999), successive dike intrusions (Nimmo, 2000), or impacts (Connerney
69 et al., 2001). This TRM can be thereafter modified by demagnetization associated with volcanoes or
70 impact craters taking place after the cessation of the dynamo (Nimmo and Gilmore, 2001). Viscous
71 remanent magnetization and demagnetization of the lower crust were also suggested by Arkani-Hamed
72 (2007) and Shahnas and Arkani-Hamed (2007). Finally, Chemical Remanent Magnetization (CRM)
73 processes may have generated the observed magnetic field anomalies. For instance, the alteration of
74 siderite ($FeCO_3$) into magnetite through magmatic intrusion in a water-rich crust can induce a
75 secondary TRM and produce water discharges that could explain the apparent correlation between

valley networks and magnetic anomalies (Harrison and Grimm, 2002).

An alternate model may be crustal CRM associated to serpentinization. This metamorphic reaction corresponds to the hydration of mafic minerals, generally producing serpentinite ($Mg_6Si_4O_{10}(OH)_8$) and other minerals such as magnetite, talc ($Mg_3Si_4O_{10}(OH)_2$) or quartz (SiO_2). Dihydrogen (H_2) is also produced and methane (CH_4) can eventually be formed if the reactant fluid contains carbon dioxide (CO_2). Serpentinization occurs at relatively low pressures (< 400 MPa) and low to medium temperatures (< 600°C). On Earth, serpentinization sites are commonly found at mid-ocean ridges, transform faults and passive margins, where shallow peridotitic mantle rocks are exhumed (Mével, 2003). Another setting is the mantle wedge of subduction where water is released from the subducted crust. In the presence of an intense magnetic field, the production of magnetite allows the mafic or ultramafic serpentinized rock to be chemically magnetized. The resulting magnetic anomalies can be large enough to be mapped at satellite altitudes on Earth (Blakely et al., 2005). Finally, serpentinization increases the rock volume, creating a relief with surrounding non-serpentinized rocks (e.g. mid-oceanic ridge elevation model of Hess, 1962)

In this paper, we investigate the serpentinization of the Noachian Martian crust to explain the observed magnetic anomalies. We first describe the reference crustal model in terms of temperature and composition as regards the gravity signal. Further we compute the expected magnetizations obtained via serpentinization. These values are compared with the Martian crustal magnetization models derived from MGS measurements. In the last part we discuss our evolution model and the new insights it brings on the early Mars, especially with respect to the paleomagnetic field.

2. Thermal and compositional crustal model for early Mars

98

99 2.1. Early evolution and thermal gradient

100

101 Based on simple considerations about the energy released by the growth process, the
102 temperature of the Martian outer crust was high during accretion since a magma ocean was likely
103 present. The depth extent of this magma ocean is not well-constrained (Reese and Solomatov, 2006).
104 Just after accretion, the temperature is controlled by the melting of iron and silicate phases and their
105 subsequent cooling. This is followed by the onset of convection in the mantle (Korenaga and Jordan,
106 2002), which quickly achieves steady-state regime, as scaling laws suggest (e.g. Breuer and Spohn,
107 2006; Stevenson, 2001). The general trend is that mantle heat flux decreases with time: rapidly during
108 the Noachian, and more modestly afterwards. We assume that degree-one convection (Roberts and
109 Zhong, 2007) produces partial melting and the source of water (Médard and Grove, 2006) beneath half
110 of the planet (see Sections 4.2 and 4.3 for discussion). Serpentinization is then possible, depending on
111 the crustal thermal gradient.

112 Assuming a given temperature at the base of the elastic thickness provides the thermal gradient.
113 The interpretation of gravity and topographic data helps to estimate the elastic thickness of the
114 lithosphere at the time the relief was formed. Values range between 15 to 30 K km^{-1} during the Early
115 Noachian and decrease down to 5 to 15 K km^{-1} at the Noachian/Hesperian limit (3.7 Ga). Choblet and
116 Sotin (2001) find a rapid decrease from 30 K km^{-1} after accretion down to 8 K km^{-1} after 500 My of
117 evolution. Their model assumes that heat is transferred by convection in the stagnant lid regime, like in
118 our model, which implies very small lateral variations in heat flux. In this case, a viscosity of 10^{21} Pa s
119 gives a gradient of 2 K km^{-1}, whereas 10^{18} Pa s gives 20 K km^{-1}. The latter value is in the range of the

120 lower bound values derived by McGovern et al. (2004) and Grott et al. (2007). For a hotter crust, the
121 trend of this gradient becomes highly non-linear, leading to a similar temperature difference in the
122 Noachian Martian crust than the linear case of our model with an upper limit of 20 K km^{-1}.
123
124 2.2. Composition, thickness and topography of the Noachian Martian crust
125
126 The Martian topographic dichotomy is similar to the ocean - continent difference on Earth. It
127 corresponds to approximately 6 km of relief between the Northern lowlands and the Southern highlands
128 (Figure 1). An intriguing aspect is that there is no significative free-air gravity anomaly (or not
129 correlated with topography) across this dichotomy (Yuan et al., 2001). The amplitude is about 0.001 m
130 s^{-2} (Figure 1), which is on the order of a free-air gravity anomaly produced by a 1 km non-compensated
131 topography contrast. It means that the 6 km Martian topography contrast is mostly compensated either
132 by different thicknesses of the same crust (known as Airy model) or by lateral variation in the
133 composition of the crust (known as Pratt model).
134 The mineralogical composition of the Martian surface has been investigated by the MGS
135 Thermal Emission Spectrometer (TES) and the MEX Observatoire pour la Minéralogie, l'Eau, les
136 Glaces et l'Activité (OMEGA) instruments. They have mapped mafic minerals - mainly pyroxenes, but
137 also localized pure olivine outcrops - over the whole surface of Mars (Bandfield et al., 2000; Bibring et
138 al., 2006; Hoefen et al., 2003; Mustard et al., 2005). In-situ measurements of the Mars Exploration
139 Rovers (MERs) Spirit and Opportunity have revealed olivine in some exposed rocks of the lowlands
140 (McSween et al., 2006). In addition, analyses of Martian SNC meteorites argue in favor of a mafic
141 composition for the Martian crust (Nyquist et al., 2001). A contrast between a Southern basaltic, and a

142 Northern andesitic crust was suggested by Bandfield et al. (2000), but this distinction was not observed
143 in the MEX OMEGA data (Mustard et al., 2005). All these observations indicate a basaltic composition
144 for the Martian crust.

145 Assuming a homogeneous basaltic layer, estimates of the crustal thicknesses are 35 km in the
146 Northern Hemisphere and 60 km in the Southern one (Wieczorek and Zuber, 2004). However, this
147 thickness contrast may not be so important in the presence of a low-density rock layer in the Southern
148 crust. Lower density serpentinized rocks can account for such a layer. Serpentine minerals have not
149 been yet clearly observed on the surface of the Southern Hemisphere, even in large crater basins which
150 should contain material of deeper serpentinized parts. But their weak reflectance (dark surface)
151 precludes their detection by remote sensing methods. Nevertheless, the detection of pure olivine
152 (Hoefen et al., 2003) and magnetite (Bertelsen et al., 2004) may suggest their presence.

153 In this study, we assume an initial basaltic homogeneous Noachian crust with constant thickness
154 (Figure 2). Then the lowest part of the Southern crust is serpentinized from its bottom toward the upper
155 parts, because of the mantle water released by partial melting (cf. Subsection 2.1). The hydrostatic
156 equilibrium is expressed by:

157

158 $$(H_s + H_b - t)\ \rho_b = H_s\ \rho_s + H_b\ \rho_b \qquad (1)$$

159

160 where H_s and H_b are the final thicknesses of the serpentinized and the non-serpentinized crusts,
161 respectively (Figure 2). A topography t is created at the surface to counterbalance the decrease in
162 density from basalts (ρ_b = 3100 kg m^{-3}) to serpentinites (ρ_s = 2600 kg m^{-3}). Such a porous rock may exist
163 even at large Martian depths, because serpentinization creates its own porosity, allowing a continuous

hydration (cf. Section 4.3). For the following calculations, lower (2200 kg m^{-3}) and higher (2800 kg m^{-3}) density values are also used. In equation (1), the Northern Hemisphere is represented on the left side, and the Southern one on the right side (Figure 2). This approach allows us to estimate what is the minimum thickness of the serpentinized layer needed to reach the hydrostatic equilibrium. As a consequence, the initial thickness of the whole crust is not crucial, the only constraint is that it has to be large enough to produce a serpentinized layer, considering the thermodynamical conditions in the early Martian crust. The thickness of the initial basaltic layer available for serpentinization, H_{bs}, is expressed by:

$$H_{bs} = H_s \rho_s / \rho_b \quad (2).$$

Then Eqn. 1 is equivalent to:

$$H_{bs} = t \rho_s / (\rho_b - \rho_s) \quad (3).$$

Given the assumed densities, a 31.2 km - thick layer must be serpentinized to explain the present contrast of surface topography between the two hemispheres (6 km). Note that this scenario shows basalts still covering the whole surface of Mars, which correlates the observations. With a Mars' mean radius of about 3390 km (as the actual one) and considering the Southern Hemisphere only, the material initially available for hydration then corresponds to 2.23×10^{18} m^3 of mafic rocks. Using other serpentinite densities of 2200 and 2800 kg m^{-3}, H_{bs} ranges from 14.7 to 56.0 km, respectively.

The base of the serpentinized layer in the lower crust depends on the stability of the serpentine

minerals. In our model, this limit needs to be deeper than 31.2 km. The thermodynamical conditions of several metamorphic reactions involving water and ultramafics are shown in Figure 3, using data from Evans and Trommsdorf (1970) and Winkler (1979). A plot of several thermal gradients between 5 and 20 K km^{-1} and using 293 K as surface temperature (as the present Terrestrial mean surface temperature) reveals that the thermal gradient must be lower than 16.5 K km^{-1} to let the serpentinization to reach 31.2 km. Otherwise, enstatite (as well as olivine for shallower depths) is stable as shown on the right panel of Figure 3. If the assumed density is 2800 kg m^{-3} (i.e. lower porosity), then the thermal gradient should be about 13 K km^{-1}, which may be too low regards as the McGovern et al. (2004) and Grott et al. (2007)'s suggested ranges. Using a lower density up to 2200 kg m^{-3}, it yields about 30 K km^{-1}. Such large values have been suggested, but the used density would imply too large porosity for these depths. Thus, a density of 2600 kg m^{-3} and H_{bs} equal to 31.2 km for a thermal gradient of 16.5 K km^{-1} is a compromised model. The latter value is consistent with the range of values we suggest in the previous Subsection 2.1. All thermodynamical conditions in favor of serpentinization in the crust of the Southern Hemisphere were thus present during Noachian (see Sections 4.1 and 4.2 for discussion), creating density variations that explain the present gravity (compensation) and topography signals across the dichotomy.

3. Martian crustal magnetization via serpentinization

The serpentinization reactions are constrained by the thermodynamical conditions, by the rock bulk composition and available water volumes, as well as by the iron content in ultramafic minerals. Table 1 shows the selected mass-balanced reactions for this study. We only considered those which

produce magnetite, where iron is exclusively stored. Therefore chrysotile is formed instead of lizardite, because the latter incorporates more iron in its structure than the former (O'Hanley and Dyar, 1993). Iron fraction in the initial olivine and pyroxene minerals varies from 5 to 30% (cf. Section 4).

For each reaction, the volume percentage of produced magnetite (Vp_{Mt}) is computed using:

$$Vp_{Mt} = 100 \cdot n_{Mt} \cdot V_{Mt} / \Sigma (n_{Prod} \cdot V_{Prod}) \quad (4)$$

with n_{Mt}, n_{Prod}, V_{Mt} and V_{Prod} representing the numbers of moles and the molar volumes (in $m^3\,mol^{-1}$) of magnetite and other solid products of each reaction, respectively.

Based on magnetic measurements of serpentinized rocks, some authors proposed a linear relation between Vp_{Mt} and the magnetic susceptibility k (Oufi et al., 2002; Toft et al., 1990). The proportionality follows:

$$k \sim 0.03 \cdot Vp_{Mt} \quad (5)$$

In this way, the magnetic susceptibility of the rocks resulting from serpentinization reactions (listed in Table 1) is determined. The magnetization M (in A m^{-1}) can be estimated from the magnetic field intensity B at the surface (in Tesla), following:

$$M = k \cdot B / \mu_0 \quad (6)$$

with μ_0 the magnetic permeability of free space ($\mu_0 = 4\pi \times 10^{-7}$ H m^{-1}). The intensity of the magnetic field 4.0 Gy ago is poorly constrained for Mars as well as for the Earth (Prévot and Perrin, 1992). On average, the intensity of the Martian remanent magnetic field is 10 to 100 times larger than the actual Terrestrial lithospheric field intensity. This implies either a stronger internal field responsible for rock magnetization at the surface, and/or a combination between a Martian lithosphere enriched in magnetic material, and bearing minerals with higher magnetic susceptibility than on Earth. For convenience, a surface magnetic field of 50 000 nT is used, to be more easily compared to Terrestrial rock magnetization (cf. Section 4). The resulting remanent magnetization intensities are shown in Table 1. They range from 2.1 to 19.8 A m^{-1}, with an average of 9.7 A m^{-1}. By comparison, a Terrestrial rock is intensely magnetized when its magnetization exceeds 5 A m^{-1}. Natural Remanent Magnetizations (NRM) of 5 to 20 A m^{-1} are typically measured on mid-ocean ridge basalts and gabbros (Fox and Opdyke, 1973), although they decrease to less than 5 A m^{-1} after a few million years due to the oxydation of magnetite into maghemite (Bleil and Petersen, 1983). Numerous studies reported that some oceanic serpentinized peridotites also possess quite large (more than 5 A m^{-1}) and stable NRM (see Oufi et al., 2002 and references therein). A more complex model may assume the serpentinization of such peridotites in the Martian lithospheric mantle. The resulting magnetization would be deeper, but the heat flux has to be lower. Other intense Terrestrial NRM are also associated with continental volcanic formations (Gunnlaugsson et al., 2006), granulite rocks (McEnroe et al., 2001), as well as serpentinites (Lienert and Wasilewski, 1979).

The newly-formed magnetite changes from a superparamagnetic to a single-domain type during CRM acquisition. This CRM is very stable over geological times, with a relaxation time much greater than 100 My. Therefore there is no reason for an alteration of this CRM since the end of the Noachian

252 period, assuming no significative thermal events have affected the Martian crust during the last 3.7 Gy.
253 On the other hand, the thermal state of the crust at the place of CRM acquisition could influence the
254 resulting CRM intensity, which should decrease with depth (Dunlop and Ozdemir, 1997). This could
255 create vertical variations of the acquired CRM intensity that our model does not take into account.
256 Alternatively, the estimated values of Table 1 may represent some averages of the total magnetization
257 inside the serpentinized layer, which only contributes to the magnetic measurements at satellite altitude.
258 Unfortunately, the current magnetization state of the Martian crust is not constrained, because
259 in-situ rock magnetization measurements do not exist. Particles of the Martian soil and atmosphere are
260 magnetic (Bertelsen et al., 2004), arguing for a significant magnetization of the Martian regolith. The
261 Martian meteorites show quite weak associated magnetizations, except Los Angeles, NWA817 and
262 NWA1068 (Rochette et al., 2001). One has thus to refer to estimations of the Martian crustal
263 magnetization derived from modeling of the MGS MAG/ER magnetic measurements. A summary of
264 the published models is presented in Table 2. It clearly shows a variety of magnetization values, from 1
265 to 60 A m^{-1}, most of the models predicting a mean crustal magnetization between 0 and 20 A m^{-1}. This
266 agrees very well with the magnetization obtained by our calculations based on chemical reactions of
267 serpentinization (Table 1). Depending on the reaction, the resulting fraction of magnetite per volume of
268 rocks ranges from 2.2 (for reaction R14) to 16.6% (for reaction R24), which is consistent with the
269 observed magnetite content in Terrestrial serpentinites (10-15%; Toft et al., 1990). Thus, in the presence
270 of an intense magnetic field, production of magnetite through serpentinization may explain the intense
271 magnetization that underwent the early crust of Mars.
272
273 4. Discussion

Our model depends on several assumptions about the early evolution of Mars. We admit that all these necessary initial conditions cannot be fully proved. On the other hand, the compatibility of these hypotheses can be discussed considering the recent observations and the numerical modeling experiments that concern this topic.

4.1. Pertinence of a stagnant lid convection regime during Noachian

The thermal gradient in the crust of Mars during Noachian resulted from the early thermal evolution of the whole planet. It is commonly assumed that, after accretion, the cooling of the magma ocean precedes the onset of mantle convection (Reese and Solomatov, 2006). During a short period, the core differentiation then buffers and homogenizes the mantle temperature with a cold layer on top. This evolution ends in a stagnant lid convection regime in the early Noachian, as suggested by Choblet and Sotin (2001). Recently, Guest and Smrekar (2007) showed that, if such a regime has occurred throughout the entire Mars' history, then a transition from a wet crust to a dry one is required at 3.5 Ga to preserve the dichotomy. The lost of the liquid water phase can be explained by serpentinization, even if, in our model, this process ends at ~4.0 Ga. The latter date also corresponds to the end of an efficient crustal production (Breuer and Spohn, 2006).

An alternative of the stagnant lid model is plate tectonics. Not only it has been proposed to explain the some magnetic anomalies (e.g. Connerney et al., 1999), but also it has been invoked to generate sufficient heat flux out of the core that drives a core convection necessary to generate a dynamo (Nimmo and Stevenson, 2000). However, surface evidences for such an episode of plate

296 tectonics are lacking (Pruis and Tanaka, 1995; Zuber, 2001) and the timing of the interpreted transition
297 to a stagnant lid regime is usually arbitrary, chosen to correlate with the apparent 500 My cessation of
298 the dynamo. The absence of plate tectonics also supports the preservation of the serpentinized layer in
299 the Martian crust through geological times which would otherwise be reduced by tectonic activity and
300 recycling. Mars' mantle overturn is another possible scenario, but Guest and Smrekar (2007) show that
301 it is strongly sensitive to the initial thermal conditions, and that such an event occurred too early in the
302 Mars' history (50 My) to produce the observed magnetic anomalies.
303
304 4.2. Hemispheric serpentinization and magnetization
305
306 The present model assumes mantle convection in the so-called stagnant lid regime. Both the
307 cooling from above and internal heating favor instabilities of the cold thermal boundary layer beneath
308 the conductive lid. Cold plumes are compensated by global upwelling of the warm mantle. Such a
309 geometry favors global partial melting between the cold plumes. In addition, Zhong and Zuber (2001)
310 and Roberts and Zhong (2007) showed that degree-one convection could be triggered at the core-mantle
311 boundary producing extensive partial melting in the head of a giant upwelling hot-plume. Such hot
312 plume may have generated a consequent magmatic activity at the surface of Mars, initiating the growth
313 of the Tharsis region. Assuming the contemporaneous serpentinization of the Southern crust (as in our
314 model), different magnetization processes in the presence of a core dynamo would be implied: TRM for
315 Tharsis volcanic rocks at surface, CRM for the serpentinized rocks in the lower crust. However, no
316 intense magnetic anomalies were mapped over the Tharsis terranes. The reason could be either a less
317 intense magnetization, or, more likely, that continuing volcanic activity subsequent to the dynamo shut-

318 off have hidden some Noachian magnetized layers. This activity at Tharsis contributed to the crustal
319 growth during Noachian and later. We exclude this contribution in our model and assume that
320 serpentinization was the only crustal growth process during the end of the Noachian period (and no
321 growth later). An alternate scenario may consist in a weak serpentinization of the Southern Hemisphere
322 lower crust, allowing the remaining crust to be gradually thicken by continuous magmatism mainly
323 during Noachian and Hesperian.

324 Excluding Tharsis and large crater basins, some areas of the Southern Hemisphere seem to be
325 demagnetized (or weakly magnetized), e.g. from the west of Hellas to the east of Argyre. This
326 contradicts our model, which assumes a CRM by serpentinization in the whole crust beneath the
327 current highlands. No surface composition differences appear between these areas and the highly
328 magnetized ones, suggesting that this demagnetization may not be of geological origin. Perhaps the
329 dynamo regime (e.g. dipolar or not, with inversions or not) played a role.

330 We also would like to emphasize that a model with a serpentinization occuring in the crust of
331 both hemispheres may be possible. In such a scenario, the whole Martian crust was magnetized by
332 hydration during Noachian. Then, when the dynamo was extinct, demagnetization events (and thinning
333 of the crust) happened in the Northern Hemisphere due to endogenic (subsequent hydrothermalism?
334 mantle uplifting?) and/or exogenic (giant impact) processes (Watters et al., 2007). However, such a
335 scenario needs to be constrained concerning the chronology of each event (before or after the end of the
336 core dynamo?) and the part of the crust affected (lower or upper crust?).

337 Finally, the hypothesis of large-scale serpentinization - as considered in our model - is not well
338 supported by terrestrial observations, which indicate specific geological settings such as the subduction
339 zones or the mid-oceanic ridges. However, our model shows ideal thermodynamical conditions in the

340 entire Noachian Martian Southern crust in favor of a possible large-scale process. Furthermore, using
341 typical hydration reaction rates at large depths (~1000 m Myr^{-1}; MacDonald and Fyfe, 1985; Ranero et
342 al., 2003), the estimated timescale for this geological event fits the lifetime of the Martian dynamo
343 (~500 Ma; cf. Section 4.4.2).
344
345 4.3. Surface vs. mantle origin for crustal water
346
347 The hydration of the Martian crust at large depths was possible since the thermodynamical
348 conditions favorized serpentinization which renews the rock porosity by reducing the volume of liquid
349 water plus solid olivine to solid chrysotile, as well as by creating cracks at small scale (O'Hanley, 1992).
350 Even at low porosity conditions, this mechanism allowed a continuous hydration since it occurs
351 preferentially along grain boundaries. Indeed, Terrestrial serpentinization sites at large crustal depths
352 are observed by seismic experiments in forearc mantle of subduction zones (Ranero et al., 2003; Xia et
353 al., 2008), as well as in the lower oceanic crust and mantle beneath slow-spreading ridges (Francis,
354 1981; Chamot-Rooke et al., 1993).
355 In our model, the water is abundant enough to alter the whole ultramafic minerals, creating 2.63
356 $\times 10^{18}$ m^3 of serpentinized crust (H_s = 37.2 km in the Southern Hemisphere; cf. Equations 1-3). Typical
357 concentration of water in serpentinites is about 12 wt% (O'Hanley and Dyar, 1993). The corresponding
358 mass of water trapped in this serpentinized crust would be equal to 8.21 $\times 10^{20}$ kg, equivalent to a
359 Martian surface ocean of about 5.6 km thickness. It means that serpentinization has stored large
360 quantities of the water released by partial melting of the upper mantle.
361 Médard and Grove (2006) estimate that more than 0.4 wt% of water can be stored inside Mars

362 during its accretion, which turns out to be about three times the amount necessary to serpentinized the
363 crust. A significant amount of water was degassed during the differentiation of the planet, forming a
364 wet atmosphere and eventually a hydrosphere. It may explain many topographical or geomorphological
365 aspects of the old Martian surfaces showing indices of liquid water runoff (e.g. Masson et al., 2001).
366 Furthermore, MEX OMEGA (Bibring et al., 2006) and MERs (Ming et al., 2006) investigations have
367 detected minerals reflecting aqueous alteration during Noachian times. Other numerical simulations of
368 Mars' thermal evolution also predict significant amount of water released at this period by mantle
369 degassing (e.g. Médard and Grove, 2006).

370 However, the nature and extension of this water reservoir remains unclear. If any wide area of
371 liquid water really existed during Noachian at the surface of Mars, then it allowed hydrothermal
372 convection in the upper crust. Oze and Sharma (2005) investigated this idea and considered a large
373 serpentinization in the current Martian crust, assuming that the water penetration may reach 25 km in
374 depth. Such hydrothermalism is likely to preserve the crustal dichotomy through geological times
375 (Parmentier and Zuber, 2007; Solomon et al., 2005). However, if a global ocean serpentinized the crust
376 from above in the two hemispheres, then no dichotomy would have been formed. And if a
377 heterogeneous serpentinization led to form the dichotomy, then the water would have immediately
378 moved toward the lowlands, stopping the serpentinization in the crust beneath the highlands. The
379 observed directions of the Noachian valley networks are northward (Masson et al., 2001). Moreover, the
380 presence of an ocean in the Northern Hemisphere was suggested to occur later, during the Hesperian
381 period (Head et al., 1999), when the cratering rate was smaller. Even if hydration of the Northern
382 Hemisphere crust might have taken place at that time, resulting magnetite did not acquire any coherent
383 magnetization since the dynamo had already stopped. Therefore the present model with a

384 serpentinization from the base of the conductive lid seems to better explain the observations and the
385 formation of the dichotomy.
386
387 4.4. The iron content, ancient core dynamo and paleo-magnetic field of Mars
388
389 Mainly two factors control the magnetization associated with the serpentinization. These are the
390 iron content of the initial phases, and the contemporaneous magnetic field. The more iron there is, and
391 the more intense the ambient field is, the larger the magnetization is. Timing constraints for the dynamo
392 shut-down are also needed to suggest that serpentinization only occured during Noachian.
393
394 4.4.1. Iron content
395
396 The serpentinization reactions listed in Table 1 use mafic minerals with iron content ranging
397 from 5 to 30%. This range is consistent with the analyses of SNC meteorites (Nyquist et al., 2001),
398 which give an iron bulk content equal to 25%. This is also compatible with the interpretation of
399 physical properties of Mars (Mocquet et al., 1996; Sohl et al., 2005). Using measurements made by the
400 MERs, McSween et al. (2006) identified iron-rich enstatite and olivine (Fo_{60-40}) in the Gusev basalts.
401 However, these rocks are thought to be of Hesperian age, younger than those which may have
402 undergone serpentinization during Noachian. Martian meteorite ALH84001 contains orthopyroxene
403 cumulate that crystallized 4.5 Ga ago. Its iron bulk content is 18.4%, with orthopyroxenes made of
404 $En_{68.8}$ (Gleason et al., 1997). These values reinforce the hypothesis about the relatively high iron bulk
405 content of the initial Martian lithosphere. Oze and Sharma (2007) mentioned that an initial iron content

406 higher than 50% is not suited for serpentinization reactions, at least considering olivine as reactant. If
407 the iron content is higher than 30%, then more magnetite is produced. Depending on the law to
408 extrapolate the values derived in Table 1, a magnetization intensity range of 30-50 A m^{-1} is expected for
409 an initial iron content of 50%. These values are still in the range of published values for the Martian
410 crustal magnetization (Table 2). However, as shown by Oze and Sharma (2007), the probability of
411 serpentinization reactions decreases from 0 to 50% of initial iron content, if olivines are the reactant. It
412 thus leads to lower amounts of magnetite, which reduces the resulting magnetization to more commonly
413 cited values, e.g. 0-20 A/m. Including more iron also affects the conditions of serpentinization
414 occurence. Winkler (1979) showed that 20% of iron in the starting mafic minerals decreases by 20 K
415 the temperature of these reactions. In this case, the crustal model presented in Figure 3 has to be
416 modified towards a lower thickness for the serpentinized layer. Nevertheless, these changes are too
417 small to significantly affect our calculations. Furthermore, the same model can be assumed using either
418 a lower thermal gradient or a surface topography contrast less important. Therefore the assumed range
419 of iron fraction in the mafic minerals is relevant.
420
421 4.4.2. Timing of the Martian core dynamo shut-down
422
423 In this study, we assume a Noachian core dynamo generated by a thermally driven core
424 convection. We prefer this scenario as it explains the apparent lack of magnetization associated with
425 post-Noachian areas. In addition, it does not require the inception of an inner core (Stevenson, 2001).
426 This idea is consistent with the current interpretation of the tidal Love number (Yoder et al., 2003), as
427 well as with high-pressure-high-temperature experimental studies (Stewart et al., 2007), that Mars has a

(partially or completely) liquid core. This also agrees with the high sulfur content (up to 14% by weight) in the Martian core inferred from SNC meteorites (Dreibus and Wänke, 1985), because the presence of sulfur lowers the liquidus temperature and prevents a solid phase in a hot core. If the content of sulfur is lower, the inner core may start to freeze. However, the convection in the core is still prone to stop due to a diminishing heat flux outward the core and into the mantle due to the reduced efficiency of mantle cooling, leading to a thermally stratified core (Breuer and Spohn, 2006). In contrast, Schubert et al. (2000) assume an entirely solid Martian core (or at least a significant inner solid shell) at present times. In their model, the onset of the magnetic field is postponed until a later stage (past ~ 4.0 Ga). However, the Noachian terranes and the >4.0 Ga old ALH84001 Martian meteorite show remanent magnetization (Weiss et al., 2002), arguing for an early dynamo in the Mars' core.

4.4.3. Intensity of the Martian paleomagnetic field

We give in Table 1 magnetization values that would be associated with serpentinization processes occuring in the presence of a 50 000 nT magnetic field, as the mean field currently observed at the actuel Earth's surface. Mafic minerals with a 20% Fe concentration lead to a 10 A m^{-1} magnetization on average, while those with 30% Fe lead to 15 A m^{-1}. These values are close to global magnetization models with a magnetized thickness of 40 km (Langlais et al., 2004; Whaler and Purucker, 2005). This may indicate that the paleomagnetic field at Mars' surface was at maximum of the order of the actual Terrestrial one.

Regardless of the nature of its driving forces, if the dynamo existed, its associated Elsasser number (Λ_E), measuring the ratio of Lorentz to Coriolis forces, is written as:

$$\Lambda_E = \sigma B^2 / \rho \Omega \qquad (7)$$

where ρ and σ are density and electrical conductivity of the core respectively, and Ω is the planetary rotation rate. B represents the magnetic field inside the core. In the so-called magnetostrophic regime, the Elsasser number is close to unity: Lorentz forces due to the motion of an electric current in the presence of a magnetic field are balanced by Coriolis forces due to the planetary rotation. Knowing ρ, σ and Ω allows to infer the strength of the magnetic field, using $B \sim (\rho \Omega/\sigma)^{0.5}$. On Earth, where $\rho \approx 12\,000$ kg m^{-3}, $\sigma \approx 5 \times 10^5$ S m^{-1} and $\Omega = 7.292 \times 10^{-5}$ s^{-1}, this scaling argument leads to a field value B_{Earth} of about 1.323×10^{-3} T. The observed field value at the CMB (i.e. outside the core) is about 500 000 nT, which corresponds to an observed Λ_E of about 0.15. The difference between the expected and observed *Elsasser* number is explained by the lithospheric field overlapping the core field for high spherical harmonic degrees, and by the absence of information about the toroidal field contribution.

The same scaling argument is applied on Mars, where $\Omega = 7.077 \times 10^{-5}$ s^{-1}. Core density is estimated to 7200 kg m^{-3} (Sohl and Spohn, 1997). To estimate the electrical conductivity inside the Martian core, we use a Wiedemann-Franz law and assume a thermal conductivity inside the Martian core equal to 40 W m^{-1}K^{-1} (Williams and Nimmo, 2004). Two-end member scenarios are considered, namely pure iron or Fe-FeS (14%wt) composition. For these two cases, the estimated mean temperature inside the Martian core is 2400 K and 1850 K, respectively (Breuer and Spohn, 2006). We obtain

electrical conductivity values ranging from 4.6 $\times 10^5$ to 6.05 $\times 10^5$ S m^{-1}, which correspond to a magnetic field strength in the Martian core between 1.052 and 0.918 $\times 10^{-3}$ T. These rough estimates show that under current conditions, the Martian magnetic field inside the core would be slightly smaller (by about 30%) of the Terrestrial one. This may not be the case 4.0 Ga ago. It is also believed that the present rotation of Mars is very similar to its primordial one (Dehant et al., 2007). On the contrary, the Earth's rotation was faster than it is today, possibly down to 13 hours (Williams, 2000). The associated magnetic field inside the Earth's core was then about 1.795 $\times 10^{-3}$ T, or 35% larger than the current day value.

Extrapolation of this core field to the surface is not straightforward, not only because of the non-visible part of the field (toroidal and lithospheric contributions), but also because the Earth's core was completely liquid (Labrosse et al., 2001). For our modeling purposes, we are going to use analogues of geomagnetic field strength determined from paleointensity measurements on Earth rocks. A caveat of our approach is that due to the metamorphic processes occurred throughout the geological time, the oldest Terrestrial rocks that have been analyzed are Archean to Early Proterozoic in age (~3.5 to 2.5 Ga), younger than 4.0 Ga. However, it is assumed that their magnetization was acquired before the inner core started to solidify. Tarduno et al. (2007) recently reported values for paleofield between 20 000 and 60 000 nT, based on the analysis of Kaapvaal pluton (South Africa). Smirnov et al. (2003) reported similar values (43 000 nT) deduced from dikes in the region of Karela, Russia.

Elsasser number predicts a paleo-geomagnetic core field that was 1.35 times larger than it is today, while paleomagnetic studies see no significant differences between current and ancient

494 geomagnetic fields. This may be due to the fact that the ratio of the toroidal to poloidal magnetic field
495 was different, as a result of the absence of the inner core. Assuming similar ratios between core field
496 and surface field on Mars and the Earth 4.0 Ga ago, a mean Earth's paleomagnetic field of 40 000 nT, a
497 Martian core field of the order of 1×10^{-3} T, a basic extrapolation predicts surface magnetic fields on
498 Mars of the order of 25 000 nT. Such low fields are within the range deduced from ALH84001, between
499 0.1 and 1 times the present-day Earth's field (Weiss et al., 2002). In our study, we assumed a value of 50
500 000 nT for an easier comparison with the Earth. Our magnetization values (Table 1) have to be divided
501 by 2, leading to a mean value of 4.35 A m^{-1}. This is consistent with values given in Table 2. For
502 instance, Langlais et al. (2004) predicted a mean and maximum magnetization of 0.8 and 12 A m^{-1},
503 respectively. This mean value is for a 40-km thick layer over the whole Martian surface. When reducing
504 the thickness to 31.2 km, and considering only the highly-magnetized Terra Sirenum and Terra
505 Cimmeria areas, the mean value is 3 A m^{-1}, very close to what we find here. This indicates that the large
506 crustal magnetization of Mars does not mean that the magnetic field was intense.
507
508 *4.5. Implications for methane release*
509
510 Methane can be produced through serpentinization when water contains CO_2, like in each
511 reaction listed in Table 1. The presence and abundance of CO_2 in crustal water depends on external and
512 internal processes. Here we assume its presence and its reaction with the dihydrogen released by
513 serpentinization. The maximum number of moles of methane produced via this process can be
514 evaluated by assuming the initial content of ultramafic minerals. Using the initial volume of crust
515 available for serpentinization (2.23×10^{18} m^3; see Section 2), the production of methane through the

516 reactions of Table 1 reaches about 10^{21} moles. This has to be regarded as a maximum value because we
517 consider that all the initial reactants are consumed. It does not compare with the less important amount
518 previously proposed (see Krasnopolsky (2006) and references therein). Despite storage in the sub-
519 surface crust via clathrates and photodissociation mechanisms, it indicates that methane, and maybe
520 other complex organic molecules, may have been present in significant amount in the Noachian
521 atmosphere.
522
523 **5. Conclusions**
524
525 In this study, the Martian topographical and magnetization dichotomy is explained by assuming
526 serpentinization of mafic rocks during the Noachian. We demonstrate that Mars underwent favorable
527 conditions for such a metamorphic process. The process proposed by our model only affects the actual
528 Southern Hemisphere, and the associated decrease in density creates a topography between the two
529 hemispheres that is consistent with the surface elevation difference of the Martian dichotomy. Therefore
530 it results no significant free-air gravity anomaly. Our scenario does not need an additional topography
531 contrast at the base of the crust. Several reactions of serpentinization produce important quantities of
532 magnetite which, in the presence of an Earth-like magnetic field, yield an associated magnetization in
533 excellent agreement with crustal magnetization values derived from MGS measurements. The results
534 also fit typical natural remanent magnetizations measured on Terrestrial serpentinites. The absence of
535 important amount of magnetite in the Northern Hemisphere crust can explain the fact that the lowlands
536 lack or display weaker magnetic anomalies at the spacecraft altitude. Our model requires a core
537 magnetic field at the time of serpentinization, and we show that the large Martian crustal magnetization

intensities do not mean that this paleo-magnetic field was intense.

To confirm that serpentinization happened during the Noachian period, several additional constraints are needed. One of these is to determine the exact thermodynamic conditions at which serpentinization can occur. Answers may come from sampling through dredging, diving and ocean drilling. Another aspect concerns the detection of serpentinized rocks in the present crust of Mars. The Compact Reconnaissance Imaging Spectrometer for Mars (CRISM) on-board Mars Reconnaissance Orbiter (MRO) has the ability to detect serpentine minerals at the Mars' surface (Murchie et al., 2007). The MRO mission is also crucial to determine the exact composition of the crust, and thereafter, combining with gravimetric data, to explain the lack of gravity contrast between the two hemispheres. Last but not least, new magnetic field measurements at lower altitudes than MGS orbits are needed. The Mars Environment and Magnetic Orbiter (MEMO) mission was proposed in this way to ESA's Cosmic Vision program 2015-2025 (Langlais et al., submitted). Not only such mission would give the first magnetic measurements around Mars since MGS, but also it is designed to study the current and past atmospheric escape.

Acknowledgments

This paper benefited from a fruitful discussion with Pr. O. Oncken.

Figure Captions

Figure 1: Average profiles of Martian topography, free-air gravity anomaly and 400 km - altitude magnetic field intensity signals across the dichotomy between -60 and 60°N. Each profile corresponds to 121 values with 1 degree interval. These values were computed at each latitude by summing the values of each longitude (1 degree interval), divided by 360, using the Mars' topography, gravity and magnetic field models of Smith et al. (1999), Yuan et al. (2001) and Langlais et al. (2004), respectively. Values above Hellas and Argyre impact basins were not taken into account. The scale for the free-air gravity anomaly is in 10^{-5} m s^{-2}, i.e. in mGal.

Figure 2: Schematic N-S cross-section of the Martian crust showing the initial (1) and final (2) compositions considered in this study. Volume masses for the serpentinized (ρ_s) and basaltic (ρ_b) crusts are 2600 and 3100 kg m^{-3}, respectively. Indices for thicknesses correspond to Equations 1-3: H_b, the thickness of the southern crust that will not be serpentinized (free parameter); H_{bs}, the thickness of the initial southern crust that will be serpentinized (31 km); H_s, the final thickness of the serpentinized crust in the Southern Hemisphere (37 km); t, the surface topography created during serpentinization (and increase of volume) of the lower crust (6 km).

Figure 3: Left: Thermodynamical equilibrium of several reactions between ultramafics and water (solid lines) and thermal gradients (dot-dashed lines) with surface temperature of 293 K. Right: The associated mineralogy in the Martian crust using a thermal gradient of 16.5 K km^{-1}. Abbreviations: Br,

578 Brucite; Ch, Chrysotile; Fo, Forsterite; Tlc, Talc; Ath, Anthophyllite; En, Enstatite; H_{bs}, thickness of the

579 initial crust that will be serpentinized (see Equation 2 and Figure 2).

580

Tables

Table 1. Serpentinization reactions considered in this study, with associated magnetization intensities.

ID	Reactions of serpentinization[a]	Magnetization[b] (A m^{-1})
R01	30 Fo_{95} + 42.5 H_2O + 0.25 CO_2 = 7.5 Ch + 1 Mt + 12 Br + 0.25 CH_4	2.7
R02	30 Fo_{90} + 40 H_2O + 0.50 CO_2 = 7.5 Ch + 2 Mt + 9 Br + 0.50 CH_4	5.5
R03	30 Fo_{85} + 37.5 H_2O + 0.75 CO_2 = 7.5 Ch + 3 Mt + 6 Br + 0.75 CH_4	8.4
R04	30 Fo_{80} + 35 H_2O + 1 CO_2 = 7.5 Ch + 4 Mt + 3 Br + 1 CH_4	11.4
R05	30 Fo_{75} + 32.5 H_2O + 1.25 CO_2 = 7.5 Ch + 5 Mt + 1.25 CH_4	14.5
R06	30 Fo_{70} + 27 H_2O + 1.5 CO_2 = 6 Ch + 6 Mt + 3 En_{100} + 1.5 CH_4	18.3
R07	15 En_{95} + 19.25 H_2O + 0.125 CO_2 = 4.75 Ch + 0.5 Mt + 11 Q + 0.125 CH_4	2.1
R08	15 En_{90} + 25.33 H_2O + 3.67 CO_2 = 4.5 Ch + 1 Mt + 12 Q + 3.67 CH_4	4.1
R09	15 En_{85} + 17.75 H_2O + 0.375 CO_2 = 4.25 Ch + 1.5 Mt + 13 Q + 0.375 CH_4	6.3
R10	15 En_{80} + 22 H_2O + 3 CO_2 = 4 Ch + 2 Mt + 14 Q + 3 CH_4	8.4
R11	15 En_{75} + 16.25 H_2O + 0.625 CO_2 = 3.75 Ch + 2.5 Mt + 15 Q + 0.625 CH_4	10.6
R12	13.5 En_{67} + 13.5 H_2O + 0.75 CO_2 = 3 Ch + 3 Mt + 15 Q + 0.75 CH_4	14.3
R13	15 Fo_{95} + 2.5 En_{85} + 23.125 H_2O + 0.1875 CO_2 = 5 Ch + 0.75 Mt + 2.75 Br + 0.1875 CH_4	3.4
R14	6 Fo_{95} + 9.9 En_{94} + 20.3 H_2O + 0.15 CO_2 = 5 Ch + 0.6 Mt + 5.8 Q + 0.15 CH_4	2.6
R15	15 Fo_{90} + 5.25 $En_{85.7}$ + 24.75 H_2O + 0.375 CO_2 = 6 Ch + 1.5 Mt + 1.5 Q + 0.375 CH_4	5.7
R16	6 Fo_{90} + 10.8 En_{89} + 20.6 H_2O + 0.3 CO_2 = 5 Ch + 1.2 Mt + 7.6 Q + 0.3 CH_4	4.9
R17	15 Fo_{85} + 6.375 En_{82} + 25.125 H_2O + 0.5625 CO_2 = 6 Ch + 2.25 Mt + 3.75 Q + 0.5625 CH_4	8.1
R18	6 Fo_{85} + 11.7 $En_{84.6}$ + 20.9 H_2O + 0.45 CO_2 = 5 Ch + 1.8 Mt + 9.4 Q + 0.45 CH_4	7.0
R19	15 Fo_{80} + 4.5 En_{67} + 21.5 H_2O + 0.75 CO_2 = 5 Ch + 3 Mt + 4 Q + 0.75 CH_4	12.3
R20	6 Fo_{80} + 9.6 En_{75} + 17.2 H_2O + 0.6 CO_2 = 4 Ch + 2.4 Mt + 9.2 Q + 0.6 CH_4	10.9
R21	24 Fo_{75} + 0.75 Fs + 26.25 H_2O + 1.125 CO_2 = 6 Ch + 4.5 Mt + 1.5 Q + 1.125 CH_4	15.7
R22	15 Fo_{75} + 5.625 En_{67} + 21.875 H_2O + 0.9375 CO_2 = 5 Ch + 3.75 Mt + 6.25 Q + 0.9375 CH_4	14.4
R23	6 Fo_{75} + 10.5 En_{71} + 17.5 H_2O + 0.75 CO_2 = 4 Ch + 3 Mt + 11 Q + 0.75 CH_4	12.8
R24	15 Fo_{70} + 3.75 En_{40} + 18.25 H_2O + 1.125 CO_2 = 4 Ch + 4.5 Mt + 6.5 Q + 1.125 CH_4	19.8
R25	6 Fo_{70} + 8.4 En_{57} + 13.8 H_2O + 0.9 CO_2 = 3 Ch + 3.6 Mt + 10.8 Q + 0.9 CH_4	18.2

[a] Abbreviations: Fo, Forsterite ($(Mg,Fe)_2SiO_4$); Ch, Chrysotile ($Mg_6Si_4O_{10}(OH)_8$); Mt, Magnetite (Fe_3O_4); Br, Brucite ($Mg(OH)_2$); En, Enstatite ($(Mg,Fe)_2Si_2O_6$); Q, Quartz (SiO_2); Fs, Ferrosillite ($Fe_2Si_2O_6$). Indices in Fo and En correspond to the magnesium content relative to iron (e.g. Fo_{75} means $(Mg_{0.75}Fe_{0.25})_2SiO_4$). Reactions R06 and R12 to R25 are in equilibrium with Br + Q = 0.5 En_{100} + water: therefore the iron content in the pyroxene differs from the one in olivine. Methane (CH_4) is formed via

589 dihydrogen (H_2) and a Fischer-Tropsch typical reaction assuming the presence of CO_2.

590 [b] Magnetization intensities are calculated via volume percentage of magnetite, magnetic susceptibility

591 and assuming a surface magnetic field during magnetization of 50 000 nT.

592

593 **Table 2.** Models of the Martian crustal magnetization derived from MGS magnetic measurements.

Authors	Crustal magnetization intensity (A m^{-1})	Depth (km)	Location[a]
Connerney et al., 1999	20	0-30	T.C.
Sprenke and Baker, 2000	20	0-30	T.C.
Connerney et al., 2001	60	0-3	T.C.
Nimmo and Gilmore, 2001	40	0-10	T.S.-T.C.
Frawley and Taylor, 2004	20	0-20	T.S.
Smrekar et al., 2004	9	0-10	I.A.
Langlais and Purucker, 2007	1 to 10	20	A.P.
Quesnel et al., 2007	> 30	> 30	T.S.
Purucker et al., 2000	0 to 20	0-50	Global
Arkani-Hamed, 2003	0 to 30	0-30	Global
Parker, 2003	> 5	0-50	Global
Langlais et al., 2004	0 to 12	0-40	Global
Whaler and Purucker, 2005	0 to 20	0-40	Global

594 [a] Abbreviations: T.C., Terra Cimmeria; T.S., Terra Sirenum; I.A., Ismenius Area; A.P., Apollinaris

595 Patera.

596

597

598 **Figures**

599

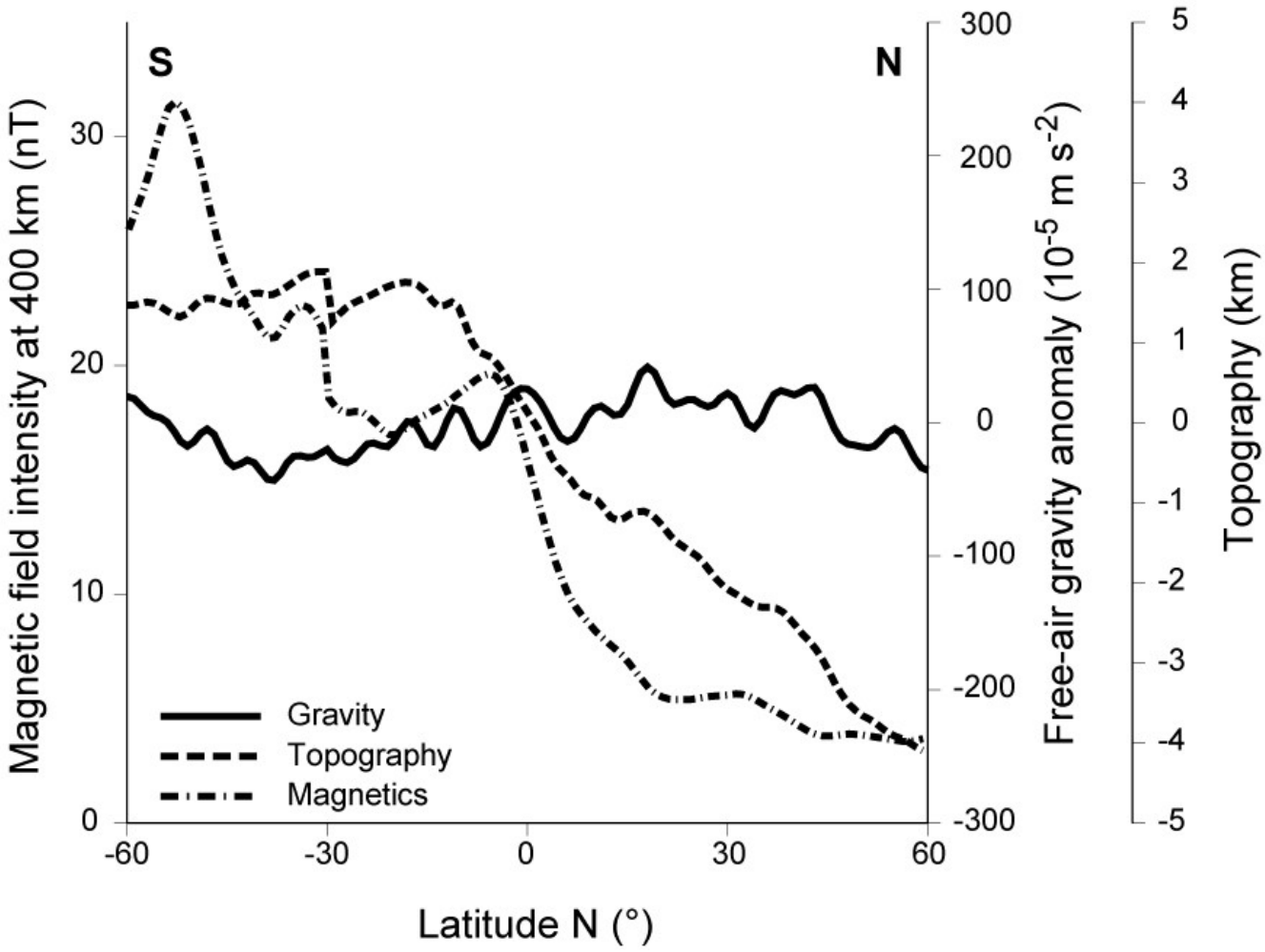

600 **Figure 1:** Average profiles of Martian topography, free-air gravity anomaly and 400 km - altitude
601 magnetic field intensity signals across the dichotomy between -60 and 60°N. Each profile corresponds
602 to 121 values with 1 degree interval. These values were computed at each latitude by summing the
603 values of each longitude (1 degree interval), divided by 360, using the Mars' topography, gravity and
604 magnetic field models of Smith et al. (1999), Yuan et al. (2001) and Langlais et al. (2004), respectively.
605 Values above Hellas and Argyre impact basins were not taken into account. The scale for the free-air

gravity anomaly is in 10^{-5} m s^{-2}, i.e. in mGal.

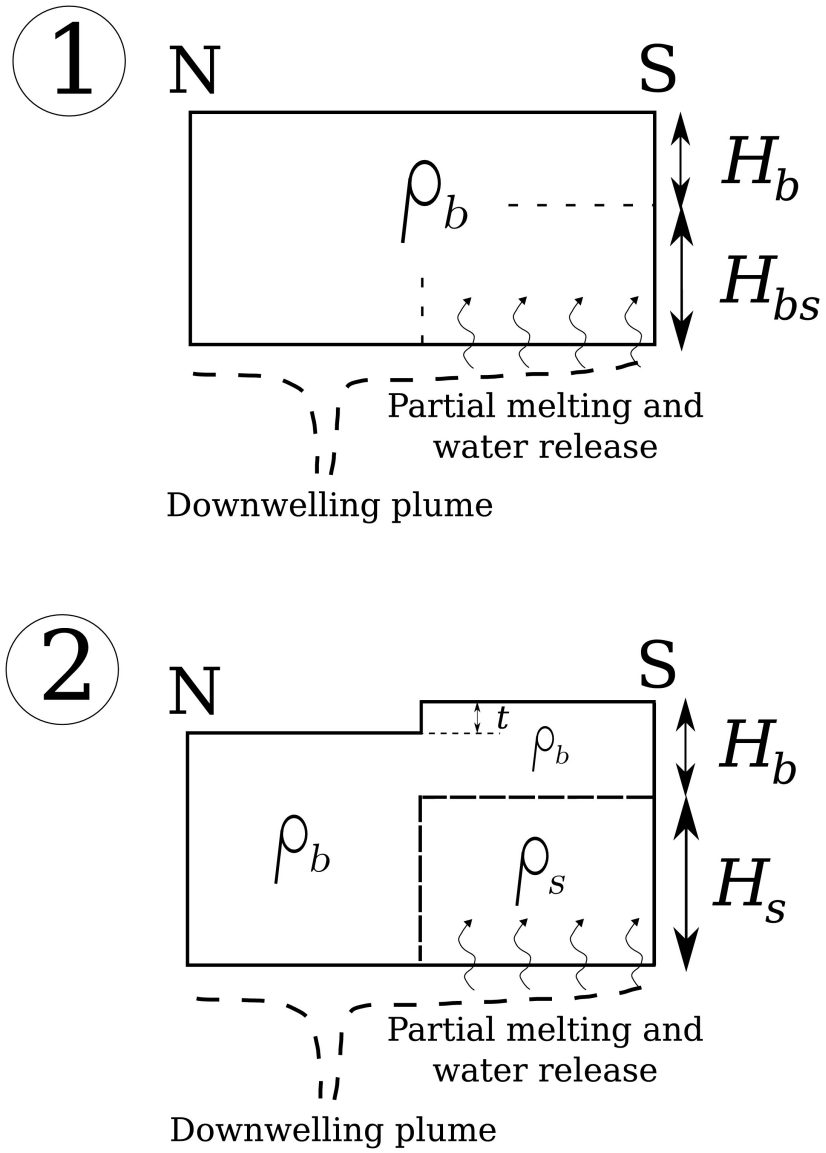

Figure 2: Schematic N-S cross-section of the Martian crust showing the initial (1) and final (2) compositions considered in this study. Volume masses for the serpentinized (ρ_s) and basaltic (ρ_b) crusts are 2600 and 3100 kg m^{-3}, respectively. Indices for thicknesses correspond to Equations 1-3: H_b, the

thickness of the southern crust that will not be serpentinized (free parameter); H_{bs}, the thickness of the initial southern crust that will be serpentinized (31 km); H_s, the final thickness of the serpentinized crust in the Southern Hemisphere (37 km); t, the surface topography created during serpentinization (and increase of volume) of the lower crust (6 km).

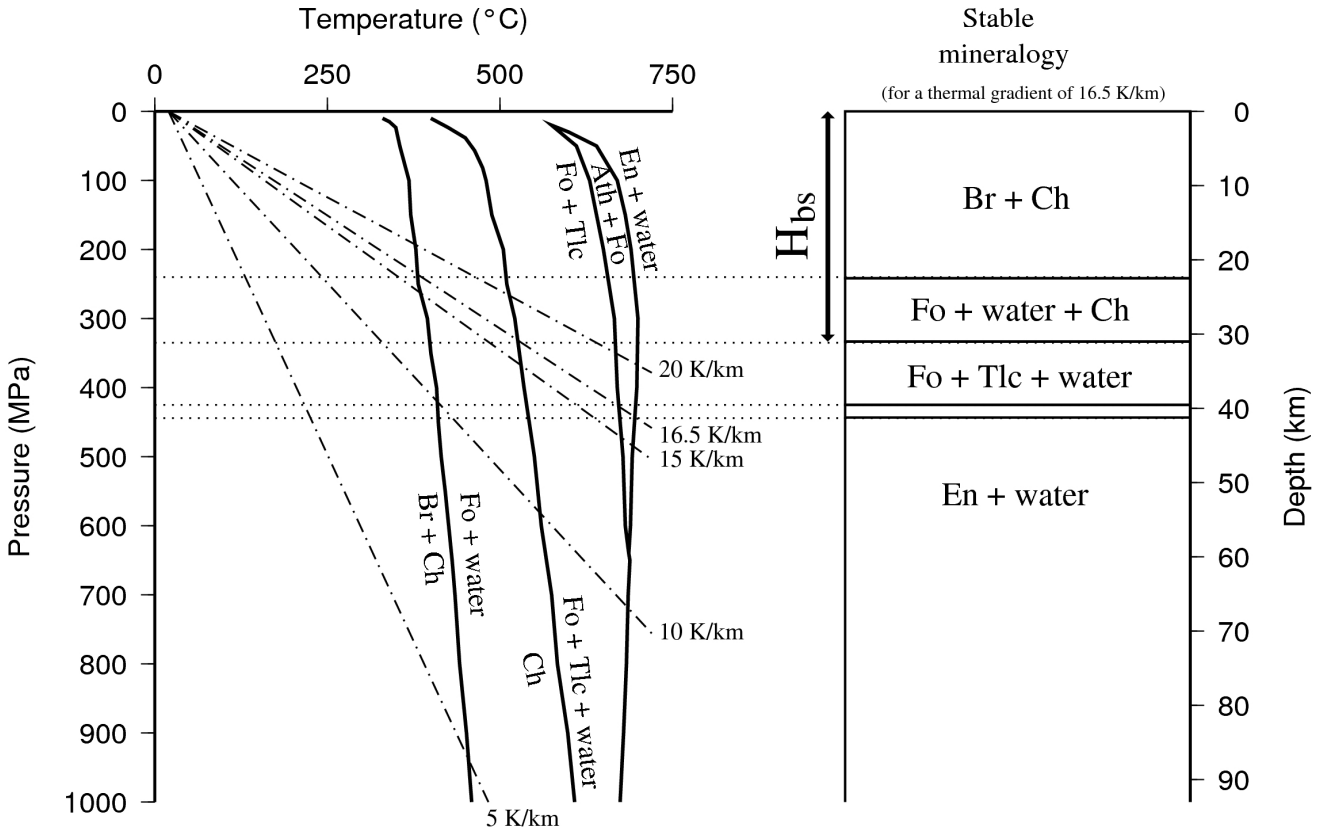

Figure 3: Left: Thermodynamical equilibrium of several reactions between ultramafics and water (solid lines) and thermal gradients (dot-dashed lines) with surface temperature of 293 K. Right: The associated mineralogy in the Martian crust using a thermal gradient of 16.5 K km^{-1}. Abbreviations: Br, Brucite; Ch, Chrysotile; Fo, Forsterite; Tlc, Talc; Ath, Anthophyllite; En, Enstatite; H_{bs}, thickness of the initial crust that will be serpentinized (see Equation 3 and Figure 2).

639 **References**

640

641 Acuña, M.H., Connerney, J.E.P., Wasilewski, P., Lin, R.P., Mitchell, D., Anderson, K.A., Carlson, C.W.,
642 McFadden, J., Rème, H., Mazelle, C., Vignes, D., Bauer, S.J., Cloutier, P., Ness, N.F., 2001.
643 Magnetic field of Mars: Summary of results from the aerobraking and mapping orbits. J.
644 Geophys. Res. 106, 23403-23417.

645 Arkani-Hamed, J., 2003. Thermoremanent magnetization of the Martian lithosphere. J. Geophys. Res.
646 108, 5114.

647 Arkani-Hamed, J., 2005. On the possibility of single-domain/pseudo-single-domain magnetic particles
648 existing in the lower crust of Mars: Source of the strong magnetic anomalies. J. Geophys. Res.
649 110, E12009, doi:10.1029/2005JE002535.

650 Arkani-Hamed, J., 2007. Magnetization of Martian lower crust: Revisited. J. Geophys. Res. 112,
651 E05008, doi:10.1029/2006JE002824 .

652 Bandfield, J.L., Hamilton, V.E., Christensen, P.R., 2000. A Global View of Martian Surface
653 Compositions from MGS-TES. Science 287, 1626-1630.

654 Bertelsen, P., Goetz, W., Madsen, M.B., Kinch, K.M., Hviid, S.F., Knudsen, J.M., Gunnlaugsson, H.P.,
655 Merrison, J., Nornberg, P., Squyres, S.W., Bell, J.F., Herkenhoff, K.E., Gorevan, S., Yen, A.S.,
656 Myrick, T., Klingelhöfer, G., Rieder, R., Gellert, R., 2004. Magnetic Properties Experiments
657 on the Mars Exploration Rover Spirit at Gusev Crater. Science 305, 827-829.

658 Bibring, J-P., Langevin, Y., Mustard, J.F., Poulet, F., Arvidson, R., Gendrin, A., Gondet, B., Mangold,
659 N., Pinet, P., Forget, F., the OMEGA team, 2006. Global Mineralogical and Aqueous Mars
660 History Derived from OMEGA/Mars Express Data. Science 312, 400-404.

661 Blakely, R.J., Brocher, T.M., Wells, R.E., 2005. Subduction-zone magnetic anomalies and
662 implications for hydrated forearc mantle. Geology 33, 445-448.
663 Bleil, U., Petersen, N., 1983. Variations in magnetization intensity and low-temperature titanomagnetite
664 oxidation of ocean floor basalts. Nature 301, 384-388.
665 Breuer, D., Spohn, T., 2006. Viscosity of the Martian mantle and its initial temperature: Constraints
666 from crust formation history and the evolution of the magnetic field. Planet. Space Sci. 54,
667 153-169.
668 Chamot-Rooke, N., Jestin, F., De Voogd, B., the Phèdre Working Group, 1993. Intraplate shortening in
669 the central Indian Ocean determined from 2100- km-long north-south deep seismic reflection
670 profile. Geology 21, 1043-1046.
671 Choblet, G., Sotin, C., 2001. Early transient cooling of Mars. Geophys. Res. Lett. 28, 3035-3038.
672 Connerney, J. E. P., Acuña, M.H., Wasilewski, P.J., Ness, N.F., Rème, H., Mazelle, C., Vignes, D., Lin,
673 R.P., Mitchell, D.L., Cloutier, P.A., 1999. Magnetic Lineations in the Ancient Crust of Mars.
674 Science 284, 794-798.
675 Connerney, J.E.P., Acuña, M.H., Wasilewski, P.J., Kletetschka, G., Ness, N.F., Rème, H., Lin, R.P.,
676 Mitchell, D.L., 2001. The Global Magnetic Field of Mars and Implications for Crustal
677 Evolution. Geophys. Res. Lett. 28, 4015-4018.
678 Dehant, V., Lammer, H., Kulikov, Y.N., Grießmeier, J.-M., Breuer, D., Verhoeven, O., Karatekin, Ö.,
679 Van Hoolst, T., Korablev, O., Lognonné, P., 2007. Planetary Magnetic Dynamo Effect on
680 Atmospheric Protection of Early Earth and Mars. Sp. Sci. Rev. 129, 279-300.
681 Dreibus, G., Wänke, H., 1985. Mars, a volatile-rich planet. Meteoritics 20, 367-381.
682 Evans, B.W., Trommsdorf, V., 1970. Regional metamorphism of ultramafic rocks in the Central Alps:

paragenesis in the system CaO-MgO-SiO_2-H_2O. Schweiz. Min. Petr. Mitt. 50, 481-492.

Fox, P.J., Opdyke, N., 1973. Geology of the Oceanic Crust: Magnetic Properties of Oceanic Rocks. J. Geophys. Res. 78, 5139-5154.

Francis, T., 1981. Serpentinization faults and their role in the tectonics of slow spreading ridges. J. Geophys. Res. 86(B12), 11616-11622.

Frawley, J.J., Taylor, P.T., 2004. Paleo-pole positions from martian magnetic anomaly data. Icarus 172, 316-327.

Gleason, J.D., Kring, D.A., Hill, D.H., Boynton, W.V., 1997. Petrography and bulk chemistry of Martian orthopyroxenite ALH84001: Implications for the origin of secondary carbonates. Geochim. Cosmochim. Acta 61, 3503-3512.

Grott, M., Hauber, E., Werner, S., Kronberg, P., Neukum, G., 2007. Mechanical modeling of thrust faults in the Thaumasia region, Mars, and implications for the Noachian heat flux. Icarus 186, 517-526.

Guest, A., Smrekar, S.E., 2007. New constraints on the thermal and volatile evolution of Mars. Phys. Earth Planet. Int. 164, 161-176.

Gunnlaugsson, H.P., Helgason, Ö., L. Kristjánsson, L., Nornberg, P., Rasmussen, H., Steinporsson, S., Weyer, G., 2006. Magnetic properties of olivine basalt: Application to Mars. Phys. Earth Planet. Int. 154, 276-289.

Harrison, K.P., Grimm, R.E., 2002. Controls on Martian hydrothermal systems: Application to valley network and magnetic anomaly formation. J. Geophys. Res. 107, doi:10.1029/2001JE001616.

Head, J.W., Hiesinger, H., Ivanov, M., Kreslavsky, M.A., Pratt, S., Thomson, B.J., 1999. Possible Ancient Oceans on Mars: Evidence from Mars Orbiter Laser Altimeter Data. Science 286,

2134-2137.

Hess, H., 1962. History of Ocean Basins. In Engel, A., James, H., Leonard, B., Petrologic studies: a volume in honor of A.F. Buddington. New York, Geological Society of America, p. 599-620.

Hoefen, T.M., Clark, R.N., Bandfield, J.L., Smith, M.D., Pearl, J.C., Christensen, P.R., 2003. Discovery of Olivine in the Nili Fossae Region of Mars. Science 302, 627-630.

Kletetschka, G., Wasilewski, P.J., Taylor, P.T., 2000. Unique thermoremanent magnetization of multidomain sized hematite: Implications for magnetic anomalies. Earth Planet. Sci. Lett. 176, 469-479.

Kletetschka, G., Ness, N.F., Connerney, J.E.P., Acuna, M.H., Wasilewski, P.J., 2005. Grain size dependent potential for self generation of magnetic anomalies on Mars via thermoremanent magnetic acquisition and magnetic interaction of hematite and magnetite. Phys. Earth Planet. Int. 148, 149-156.

Korenaga, J., Jordan, T.H., 2002. Onset of convection with temperature- and depth-dependent viscosity. Geophys. Res. Lett. 29, doi:10.1029/2002GL015672.

Krasnopolsky, V.A., 2006. Some problems related to the origin of methane on Mars. Icarus 180, 359-367.

Labrosse, S., Poirier, J.-P., Le Mouël, J.-L., 2001. The age of the inner core. Earth Planet Sci. Lett. 190, 111-123.

Langlais, B., Purucker, M.E., 2007. A polar magnetic paleopole associated with Apollinaris Patera, Mars. Planet. Space Sci. 55, 270-279.

Langlais, B., Purucker, M.E., Mandea, M., 2004. Crustal magnetic field of Mars. J. Geophys. Res. 109. doi:10.1029/2003JE002048 (E02008).

727 Langlais, B., Leblanc, F., Fouchet, T., Barabash, S., Breuer, D., Chassefière, E., Coates, A., Dehant, V.,
728 Forget, F., Lammer, H., Lewis, S., Lopez-Valverde, M., Mandea, M., Menvielle, M., Pais, A.,
729 Paetzold, M., Read, P., Sotin, C., Tarits, P., Vennerstrom, S. Mars Environment and Magnetic
730 Orbiter model payload. Submitted to Experimental Astronomy.
731 Lienert, B.R., Wasilewski, P.J., 1979. A magnetic study of the serpentinization process at Burro
732 Mountain, California. Earth Planet Sci. Lett. 43, 406-416.
733 MacDonald, A., Fyfe, W., 1985. Rate of serpentinization in seafloor environments. Tectonophysics
734 116, 123-135.
735 Masson, P., Carr, M.H., Costard, F., Greeley, R., Hauber, E., Jaumann, R., 2001. Geomorphologic
736 evidence for liquid water. Space Sci. Rev. 96, 333-364.
737 McEnroe, S.A., Harrison, R.J., Robinson, P., Golla, U., Jercinovic, M., 2001. Effect of fine-scale
738 microstructures in titanohematite on the acquisition and stability of natural remanent
739 magnetization in granulite facies metamorphic rocks, southwest Sweden: Implications for
740 crustal magnetism. J. Geophys. Res. 106, 30523-30546.
741 McGovern, P., Solomon, S., Smith, D., Zuber, M., Simons, M., Wieczorek, M., Phillips, R., Neumann,
742 G., Aharonson, O., Head, J., 2004. Correction to "Localized gravity/topography admittance and
743 correlation spectra on Mars: Implications for regional and global evolution". J. Geophys. Res.
744 109 (E07007), doi:10.1029/2004JE002286.
745 McSween, H.Y., Wyatt, M.B., Gellert, R., Bell III, J.F., Morris, R.V., Herkenhoff, K.E., Crumpler, L.S.,
746 Milam, K.A., Stockstill, K.R., Tornabene, L.L., Arvidson, R.E., Bartlett, P., Blaney, D., Cabrol,
747 N.A., Christensen, P.R., Clark, B.C., Crisp, J.A., Des Marais, D.J., Economou, T., Farmer, J.D.,
748 Farrand, W., Ghosh, A., Golombek, M., Gorevan, S., Greeley, R., Hamilton, V.E., Johnson,

749 J.R., Joliff, B.L., Klingelhöfer, G., Knudson, A.T., McLennan, S., Ming, D., Moersch, J.E.,
750 Rieder, R., Ruff, S.W., Schröder, C., de Souza Jr., P.A., Squyres, S.W., Wänke, H., Wang, A.,
751 Yen, A., Zipfel, J., 2006. Characterization and petrologic interpretation of olivine-rich basalts at
752 Gusev Crater, Mars. J. Geophys. Res. 111. doi:10.1029/2005JE002477 (E02S10).
753 Médard, E., Grove, T.L., 2006. Early hydrous melting and degassing of the Martian interior. J.
754 Geophys. Res. 111. doi:10.1029/2006JE002742 (E11003).
755 Mével, C., 2003. Serpentinization of abyssal peridotites at mid-ocean ridges. C. R. Geoscience 335,
756 825-852.
757 Ming, D.W., Mittlefehldt, D.W., Morris, R.V., Golden, D.C., Gellert, R., Yen, A., Clark, B.C., Squyres,
758 S.W., Farrand, W.H., Ruff, S.W., Arvidson, R.E., Klingelhöfer, G., McSween, H.Y., Rodionov,
759 D.S., Schröder, C., de Souza, P.A., Wang, A., 2006. Geochemical and mineralogical indicators
760 for aqueous processes in the Columbia Hills of Gusev crater, Mars. J. Geophys. Res. 111.
761 doi:10.1029/2005JE002560 (E02S12).
762 Mocquet, A., Vacher, P., Grasset, O., Sotin, C., 1996. Theoretical seismic models of Mars: the
763 importance of the iron content of the mantle. Planet. Space Sci. 44, 1251-1268.
764 Morris, R.V., Ming, D.W., Graff, T.G., Arvidson, R.E., Bell III, J.F., Squyres, S.W., Mertzman, S.A.,
765 Gruener, J.E., Golden, D.C., Le, L., Robinson, G.A., 2005. Hematite spherules in basaltic
766 tephra altered under aqueous, acid-sulfate conditions on Mauna Kea volcano, Hawaii: Possible
767 clues for the occurrence of hematite-rich spherules in the Burns formation at Meridiani Planum,
768 Mars. Earth Planet. Sci. Lett. 240, 168-178.
769 Murchie, S., Arvidson, R., Bedini, P., Beisser, K., Bibring, J.-P., Bishop, J., Boldt, J., Cavender, P.,
770 Choo, T., Clancy, R.T., Darlington, E.H., Des Marais, D., Espiritu, R., Fort, D., Green, R.,

771 Guinness, E., Hayes, J., Hash, C., Heffernan, K., Hemmler, J., Heyler, G., Humm, D.,
772 Hutcheson, J., Izenberg, N., Lee, R., Lees, J., Lohr, D., Malaret, E., Martin, T., McGovern, J.A.,
773 McGuire, P., Morris, R., Mustard, J., Pelkey, S., Rhodes, E., Robinson, M., Roush, T., Schaefer,
774 E., Seagrave, G., Seelos, F., Silverglate, P., Slavney, S., Smith, M., Shyong, W.-J., Strohbehn,
775 K., Taylor, H., Thompson, P., Tossman, B., Wirzburger, M., Wolff, M., 2007. Compact
776 Reconnaissance Imaging Spectrometer for Mars (CRISM) on Mars Reconnaissance Orbiter
777 (MRO). J. Geophys. Res. 112. doi:10.1029/2006JE002682 (E05S03).
778 Mustard, J.F., Poulet, F., Gendrin, A., Bibring, J.-P., Langevin, Y., Gondet, B., Mangold, N., Belluci,
779 G., Altieri, F., 2005. Olivine and Pyroxene Diversity in the Crust of Mars. Science 307, 1594-1597.
780 Nimmo, F., 2000. Dike intrusion as a possible cause of linear Martian magnetic anomalies. *Geology*
781 28, 391-394.
782 Nimmo, F., Stevenson, D., 2000. Influence of early plate tectonics on the thermal evolution and
783 magnetic field of Mars. J. Geophys. Res. 105, 11969-11979.
784 Nimmo, F., Gilmore, M.S., 2001. Constraints on the depth of magnetized crust on Mars from impact
785 craters. J. Geophys. Res. 106, 12315-12323.
786 Nyquist, L.E., Bogard, D.D., Shih, C.-Y., Greshake, A., Stöffler, D., Eugster, O., 2001. Ages and
787 geologic histories of martian meteorites. Space Sci. Rev. 96, 105-164.
788 O'Hanley, D.S., 1992. Solution to the volume problem in serpentinization. Geology 20, 705-708.
789 O'Hanley, D.S., Dyar, M.D., 1993. The composition of lizardite *1T* and the formation of magnetite in
790 serpentinites. Am. Min. 78, 391-404.
791 Oufi, O., Cannat, M., Horen, H., 2002. Magnetic properties of variably serpentinized abyssal
792 peridotites. J. Geophys. Res. 107. doi:10.1029/2001JB000549.

793 Oze, C., Sharma, M., 2005. Have olivine, will gas: Serpentinization and the abiogenic production of
794 methane on Mars. Geophys. Res. Lett. 32. doi:10.1029/2005GL022691 (L10203).
795 Oze, C., Sharma, M., 2007. Serpentinization and the inorganic synthesis of H_2 in planetary surfaces.
796 Icarus 86, 557-561.
797 Parker, R.L., 2003. Ideal bodies for Mars magnetics. J. Geophys. Res. 108. doi:10.1029/2001JE001760.
798 Parmentier, E.M., Zuber, M.T., 2007. Early evolution of Mars with mantle compositional stratification
799 or hydrothermal crustal cooling. J. Geophys. Res. 112. doi:10.1029/2005JE002626 (E02007).
800 Prévot, M., Perrin, M., 1992. Intensity of the Earth's magnetic field since Precambrian from Thellier-
801 type palaeointensity data and inferences on the thermal history of the core.
802 Geophys. J. Int. 108, 613-620. doi:10.1111/j.1365-246X.1992.tb04640.x.
803 Pruis, M.J., Tanaka, K.L., 1995. The Martian Northern plains did not result from plate tectonics. *Lunar*
804 *and Planetary Science XXVI*, 1147-1148.
805 Purucker, M., Ravat, D., Frey, H., Voorhies, C., Sabaka, T., Acuna, M., 2000. An altitude-normalized
806 magnetic map of Mars and its interpretation. Geophys. Res. Lett. 27, 2449-2452.
807 Quesnel, Y., Langlais, B., Sotin, C., 2007. Local inversion of magnetic anomalies: Implication for
808 Mars' crustal evolution. Planet. Space Sci. 55, 258-269.
809 Ranero, C., Phipps Morgan, J., McIntosh, K., Reichert, C., 2003. Bending-related faulting and mantle
810 serpentinization at the Middle America trench. Nature 425, 367-373.
811 Reese, C.C., Solomatov, V.S., 2006. Fluid dynamics of local martian magma oceans. Icarus 184, 102-
812 120.
813 Roberts, J.H., Zhong, S., 2007. The cause for the north-south orientation of the crustal dichotomy and
814 the equatorial location of Tharsis on Mars. Icarus 190, 24-31.

815 Rochette, P., Lorand, J.-P., Fillion, G., Sautter, V., 2001. Pyrrhotite and the remanent magnetization of
816 SNC meteorites: a changing perspective on Martian magnetism. Earth Planet. Sci. Lett. 190, 1-
817 12.
818 Schubert, G., Russell, C.T., Moore, W.B., 2000. Timing of the Martian dynamo. Nature 408, 666-667.
819 Shahnas, H., Arkani-Hamed, J., 2007. Viscous and impact demagnetization of Martian crust. J.
820 Geophys. Res. 112. doi:10.1029/2005JE002424 (E02009).
821 Smirnov, A.V., Tarduno, C.J., Pisakin, B.N., 2003. Paleointensity of the early geodynamo (2.45 Ga) as
822 recorded in Karelia: A single-crystal approach. Geology 31, 415-418.
823 Smith, D.E., Zuber, M.T., Solomon, S.C., Phillips, R.J., Head, J.W., Garvin, J.A., Banerdt, W.B.,
824 Muhleman, D.O., Pettengill, G.H., Neumann, G.A., Lemoine, F.G., Abshire, J.B., Aharonson,
825 O., Brown, C.D., Hauck, S.A., Ivanov, A.B., McGovern, P.J., Zwally, H.J., Duxbury, T.C., 1999.
826 The Global Topography of Mars and Implications for Surface Evolution. Science 284, 1495-
827 1503.
828 Smrekar, S.E., McGill, G.E., Raymond, C.A., Dimitriou, A.M., 2004. Geologic Evolution of the
829 Martian dichotomy in the Ismenius area of Mars and implications for plains magnetization. J.
830 Geophys. Res. 109. doi:10.1029/2004JE002260 (E11002).
831 Sohl, F., Spohn, T., 1997. The interior structure of Mars: Implications from SNC meteorites. J.
832 Geophys. Res. 102, 1613-1635.
833 Sohl, F., Schubert, G., Spohn, T., 2005. Geophysical constraints on the composition and structure of
834 the Martian interior. J. Geophys. Res. 110. doi:10.1029/2005JE002520 (E12008).
835 Solomon, S.C., Aharonson, O., Aurnou, J., Banerdt, W.B., Carr, M.H., Dombard, A.J., Frey, H.V.,
836 Golombek, M.P., Hauck II, S.A., Head III, J.W., Jakosky, B.M., Johnson, C.L., McGovern, P.J.,

837 Neumann, G.A., Phillips, R.J., Smith, D.E., Zuber, M.T., 2005. New Perspectives on Ancient
838 Mars. Science 307, 1214-1220.
839 Sprenke, K.F., Baker, L.L., 2000. Magnetization, Paleomagnetic Poles, and Polar Wander on Mars.
840 Icarus 147, 26-34.
841 Stevenson, D.J., 2001. Mars' core and magnetism. Nature 412, 214-219.
842 Stewart, A.J., Schmidt, M.W., van Westrenen, W., Liebske, C., 2007. Mars: A New Core-Crystallisation
843 Regime. Science 316, 1323-1325.
844 Tarduno, J.A., Cottrell, R.D., Watkeys, M.K., Bauch, D., 2007. Geomagnetic field strength 3.2 billion
845 years ago recorded by single silicate crystals. Nature 446, 657-660.
846 Toft, P.B., Arkani-Hamed, J., Haggerty, S.E., 1990. The effects of serpentinization on density and
847 magnetic susceptibility: a petrophysical model. Phys. Earth Planet. Int. 65, 137-157.
848 Watters, T.R., McGovern, P.J., Irwin III, R.P., 2007. Hemispheres Apart: The Crustal Dichotomy on
849 Mars. Annu. Rev. Earth Planet. Sci. 35, 621-652.
850 Weiss, B.P., Vali, H., Baudenbacher, F.J., Kirschvink, J.L., Stewart, S.T., Schuster, D.L., 2002. Record
851 of an ancient Martian magnetic field in ALH84001. Earth Planet. Sci. Lett. 201, 449-463.
852 Whaler, K.A., Purucker, M.E., 2005. A spatially continuous magnetization model for Mars. J.
853 Geophys. Res. 110. doi :10.1029/2004JE002393 (E09001).
854 Wieczorek, M.A., Zuber, M.T., 2004. Thickness of the Martian crust: Improved constraints from geoid-
855 to-topography ratios. J. Geophys. Res. 109. doi:10.1029/2003JE002153 (E01009).
856 Williams, G.E., 2000. Geological constraints on the Precambrian history of Earth's rotation and the
857 Moon's orbit. Rev. Geoph. 38, 37-59.
858 Williams, J.-P., Nimmo, F., 2004. Thermal evolution of the Martian core: Implications for an early

dynamo. Geology 32, 97-100.

Winkler, H.G.F., 1979. Petrogenesis of Metamorphic Rocks, fifth ed. Springer-Verlag, New York, Heidelberg, Berlin.

Xia, S., Zhao, D., Qiu, X., 2008. Tomographic evidence for the subducting oceanic crust and forearc mantle serpentinization under Kyushu, Japan. Tectonophysics 449, 85-96.

Yoder, C.F., Konopliv, A.S., Yuan, D.N., Standish. E.M., Folkner, W.M., 2003. Fluid Core Size of Mars from Detection of the Solar Tide. Science 300, 299-303.

Yuan, D., Sjogren, W.L., Konopliv, A.S., Kucinskas, A.B., 2001. Gravity field of Mars: A 75th Degree and Order Model. J. Geophys. Res. 106, 23377-23402.

Zhong, S., Zuber, M.T., 2001. Degree-1 mantle convection and the crustal dichotomy on Mars. Earth Planet Sci. Lett. 189, 75-84.

Zuber, M.T., 2001. The crust and mantle of Mars. Nature 412, 220-227.